

Spontaneous polarization driven Mg concentration profile reconstruction in MgZnO/ZnO heterostructures

Cite as: Appl. Phys. Lett. **104**, 242112 (2014); <https://doi.org/10.1063/1.4884383>

Submitted: 25 April 2014 . Accepted: 09 June 2014 . Published Online: 19 June 2014

K. Imasaka, J. Falson, Y. Kozuka, A. Tsukazaki, and M. Kawasaki



View Online



Export Citation



CrossMark

ARTICLES YOU MAY BE INTERESTED IN

[Electron scattering times in ZnO based polar heterostructures](#)

Applied Physics Letters **107**, 082102 (2015); <https://doi.org/10.1063/1.4929381>

[Challenges and opportunities of ZnO-related single crystalline heterostructures](#)

Applied Physics Reviews **1**, 011303 (2014); <https://doi.org/10.1063/1.4853535>

[Precise calibration of Mg concentration in \$\text{Mg}_x\text{Zn}_{1-x}\text{O}\$ thin films grown on ZnO substrates](#)

Journal of Applied Physics **112**, 043515 (2012); <https://doi.org/10.1063/1.4748306>

Lock-in Amplifiers
Find out more today



Zurich
Instruments



Spontaneous polarization driven Mg concentration profile reconstruction in MgZnO/ZnO heterostructures

K. Imasaka,¹ J. Falson,¹ Y. Kozuka,^{1,a)} A. Tsukazaki,^{2,3} and M. Kawasaki¹

¹Department of Applied Physics and Quantum-Phase Electronics Center (QPEC), University of Tokyo, Tokyo 113-8656, Japan

²Institute for Materials Research, Tohoku University, Sendai 980-8577, Japan

³PRESTO, Japan Science and Technology Agency (JST), Chiyoda-ku, Tokyo 102-0075, Japan

(Received 25 April 2014; accepted 9 June 2014; published online 19 June 2014)

Atomic reconstruction at the interface of MgZnO and ZnO in molecular beam epitaxy grown heterostructures is investigated. Using secondary ion mass spectroscopy, we experimentally find that Mg atomic reconstruction depends on the polarity of the interface; it is not observed in *n*-type interfaces (MgZnO on Zn-polar ZnO) owing to electron accumulation, while in *p*-type interfaces (ZnO on Zn-polar MgZnO), Mg drastically redistributes into the ZnO layer. Combined with self-consistent calculation of band profiles and carrier distributions, we reveal that the observed Mg reconstruction is not due to thermal diffusion but consequences in order to avoid hole accumulation. This tendency implies inherent significant asymmetry of energy scales of atomic and electronic reconstructions between *n*-type and *p*-type interfaces. © 2014 AIP Publishing LLC. [<http://dx.doi.org/10.1063/1.4884383>]

Atomic and electronic reconstructions at semiconductor interfaces are subjects of great fundamental importance in designing operational devices due to the sensitivity of junction properties to local structures.^{1–3} Recent rapid progress in oxide thin film growth has enabled the precise investigation of these issues at oxide interfaces, and has revealed that unique reconstruction mechanisms are active.^{4–7} One prominent examples is the (001) LaAlO₃/SrTiO₃ interface, where alternating stacking of (LaO)⁺ and (AlO₂)[−] layers in LaAlO₃ and (SrO)⁰ and (TiO₂)⁰ in SrTiO₃ results in an electrostatically unstable interface due to the polar discontinuity leading to potential divergence.^{4,5}

In addition to the above example of a polar/non-polar interface, a mismatch of spontaneous polarization at hetero-interfaces results in a similar electrostatic instability.^{8–10} When two noncentrosymmetric materials possessing different polarization values are intimately contacted, a discontinuity of polarization ΔP inevitably resides at the interface, giving rise to potential divergence without relaxation as depicted in Fig. 1(a). An accessible crystal structure to realize such interface is the Wurtzite type, with representative materials of BeO, GaN, and ZnO, where anions and cations are tetrahedrally coordinated to each other but slightly shifted from the center of gravity due to partial ionicity.^{11,12} Importantly, in such structures, the (0001) and (000 $\bar{1}$) surfaces of this crystal are terminated by one of the species of the atoms depending on the crystal direction. In the case of ZnO, this is Zn termination for the (0001) surface and O termination for the (000 $\bar{1}$) surface.¹³ Owing to this feature, it is, thus, possible to avoid mixed termination problems as often seen in perovskite materials, where, for example, SrO or TiO₂ termination is easily mixed at the surface of SrTiO₃, sensitively depending on surface preparation.¹⁴

The Wurtzite type MgZnO/ZnO heterostructure is a promising technological platform as evidenced efficient ultraviolet light emission observed in *p*-MgZnO/*n*-ZnO junctions.^{15–20} In similar heterostructures, high electron mobility transistors have been fabricated through the formation of two-dimensional (2D) electrons at the MgZnO/ZnO

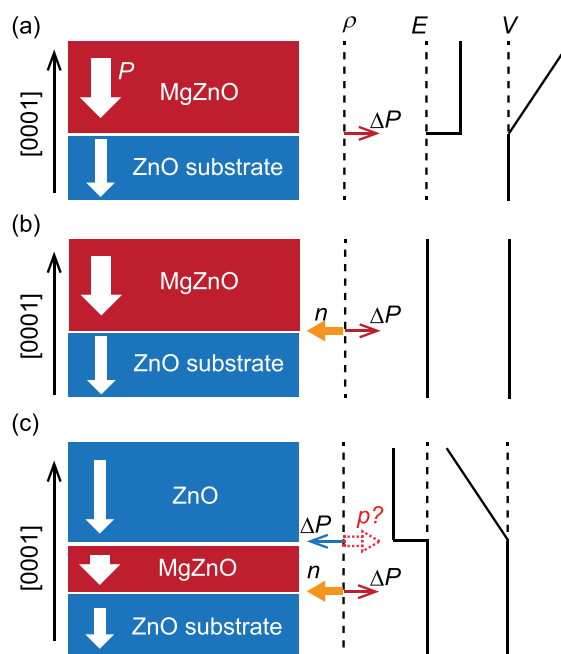


FIG. 1. (a) Schematic diagram of MgZnO on Zn-polar ZnO substrate, forming *n*-type interface. Corresponding charge density (ρ), electric field (E), and potential (V) are also depicted. (b) The same structure with including electronic reconstruction by electron accumulation. (c) Schematic diagram for additional MgZnO layer grown on the structure of (a), forming *p*-type interface. Hole accumulation in question is also depicted. For all cases, we assumed a flat potential in the ZnO substrate owing to appropriate charge compensation by charged adsorbents at the back of the substrate, while any compensation was assumed at the surface of films, which are not drawn here.

^{a)}Author to whom correspondence should be addressed. Electronic mail: kozuka@ap.t.u-tokyo.ac.jp

heterointerface,^{21–23} where the electron mobility of the high-quality samples now reaches $800\,000\text{ cm}^2\text{ V}^{-1}\text{ s}^{-1}$ (Ref. 24). It is now well established that the 2D electron gas (2DEG) is formed as a result of electronic reconstruction to relax the polarization discontinuity between MgZnO and ZnO with the relation $\Delta P/e \approx n_{2D}$ ($1.5 \times 10^{11}\text{ cm}^{-2}$ per 1% Mg), where e is the elementary electric charge and n_{2D} is the sheet carrier density of the 2DEG [Fig. 1(b)] holding well across a wide range of Mg concentrations.^{23–25} Although electric properties have been studied extensively at this Zn-polar single heterointerface, atomic reconstruction details remains less well understood.

In this study, we investigate atomic reconstructions in various types of thin film heterostructures composed of MgZnO and ZnO layers. As introduced above, the polarity of heterointerface is solely determined by the growth direction and the stacking sequence of MgZnO and ZnO; an *n*-type (*p*-type) interface is formed for MgZnO (ZnO) layer on Zn-polar ZnO (MgZnO) layer because positive (negative) polarization charges difference ΔP remain at the interface [Fig. 1(c)]. For a range of structures, the concentration profile of Mg is selectively measured as a function of depth using secondary ion mass spectroscopy (SIMS). We find the Mg profile is sharp and well defined in the case of *n*-type interface, while significant invasion of Mg into the ZnO layer from MgZnO is observed in the *p*-type interface. Since Mg concentration is a determinant factor for the magnitude of polarization charges dP/dx (P is the polarization and x is the coordinate along growth direction), experimental results are compared with potential profile calculations. This clarifies that the observed behavior cannot be explained by thermal diffusion but is instead interpreted as the avoidance of the accumulation of high-density holes. Our result indicates drastic asymmetry in the energy scales of electronic and atomic reconstructions between *n*-type and *p*-type interfaces in this material.

All films were fabricated by molecular beam epitaxy (MBE) on Zn-polar ZnO single-crystal substrates (Tokyo Denpa Co.)²⁶ with 50 nm-thick ZnO buffer layers at 850°C using high-purity metal sources of Zn (7N5) and Mg (6N), and distilled ozone. Prior to growth, the substrates were etched by HCl for 30 second and annealed in the vacuum chamber at 915°C for 15 min.²⁷ The growth rate was fixed at 600 nm/h. Surface morphology and crystallinity were

characterized by atomic force microscopy and x-ray diffraction, respectively, which showed atomically flat surfaces and the high quality of the films with the in-plane lattice fixed to the substrate.²⁸ We set the Mg content of MgZnO layer to be 20% for all samples with no sign of MgO segregation, as measured by x-ray diffraction.²⁹ Mg profiles were measured by SIMS (Fig. 2), and band and carrier profiles were calculated using the simulation program nextnano3 (Ref. 30).

We begin by fabricating Sample A, an *n*-type interface comprised of a 450 nm-thick MgZnO layer on ZnO buffer/ZnO substrate. The design (dotted line) and measured (red solid line) Mg profile is shown in Fig. 2. As expected, the SIMS measurement for this sample indicates that the interface is sharp, as per design. In this sample, electronic reconstruction occurs by forming 2D electrons at the interface as observed in earlier studies,^{9,24} and hence atomic reconstruction is not needed. We now add to this structure *p*-type interfaces by growing ZnO on top of the MgZnO layer. Sample B is formed by growing a 10 nm-thick ZnO layer on top of 100 nm-thick MgZnO layer and evidently, both interfaces remain intact. In fact, the potential decrease at the surface from the *p*-type interface is estimated as 0.33 eV (based on the uncompensated charge density at the interface of $\Delta P = 0.48\text{ }\mu\text{C}/\text{cm}^2$ for Mg = 20%),²⁵ which is much smaller than the band gap. Thus, no reconstruction is necessary at this thickness of the top ZnO layer. However, by increasing the thickness of the capping ZnO layer to 50 nm (Sample C), the Mg profile begins to show a severely distorted distribution compared with the design, and particularly so at the *p*-type interface. This effect is further enhanced by growing even thicker ZnO (300 nm) on MgZnO (Sample D), leading to abrupt drop of Mg content deep within the MgZnO layer, followed by a nearly linear gradient of Mg distribution towards to the surface.

This experimental result could immediately invoke the interpretation of thermal diffusion playing a dominant role. However, the profile differs significantly from an error function type distribution which would be expected from the diffusion equation.³¹ Further support discounting the thermal diffusion scenario is observed in Sample E, where a 100 nm-thick MgZnO is grown on 10 nm ZnO. Here, Mg is distributed as designed and a thin ZnO layer is maintained. These results indicate that the unexpected Mg redistribution is rather due to an inherent asymmetry of reconstruction

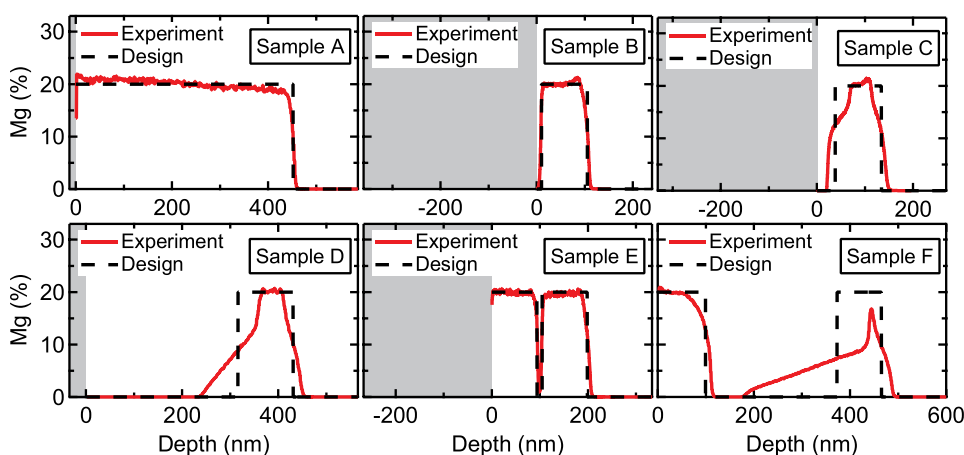


FIG. 2. SIMS depth profiles of Mg concentration for Sample A to Sample F. The solid curves are experimentally detected Mg profiles, and the dashed curves are the designed Mg profile. The surface is set to be 0 nm.

mechanisms between *n*-type and *p*-type interfaces. This hypothesis is further supported by growing additional 100 nm-thick MgZnO layer on top of 300 nm-thick ZnO (Sample F), where we find both of the *n*-type interface to be stable against atomic reconstruction, even when it is situated above the Mg-redistributed *p*-type interface. This leads to the surprising observation; Mg seems to distribute at *p*-type interfaces but ceases its advance when an *n*-type interface is formed. The different Mg distributions in the ZnO layers observed in Samples D and F may originate from a difference in growth duration resulting from the inclusion of the top MgZnO layer as in Sample F. However, the addition of this second *n*-type interface suggests that while Mg distributes drastically at all *p*-type interfaces, its advance is apparently halted when an *n*-type interface is in close proximity. In spite of this slight quantitative effect of growth time, the array of tendencies observed across the presented samples clearly indicates that a peculiar and complex reconstruction mechanism of Mg in MgZnO/ZnO is at work.

In order to understand the Mg redistribution from an electronic viewpoint, calculations of the band profile and carrier distributions were performed by employing the self-consistent Poisson-Schödinger equation expressed as³²

$$\frac{d^2}{dx^2}V = -\frac{\rho}{\epsilon}, \quad (1)$$

$$\frac{d^2}{dx^2}\psi + \frac{2m^*}{\hbar^2}(E - V) = 0, \quad (2)$$

where V is the potential, ρ is the charge density, ϵ is the dielectric constant, ψ is the wavefunction of carriers, m^* is the effective mass of electrons or holes, and \hbar is the Planck constant divided by 2π . Here, ρ is the sum of carrier distribution $|\psi|^2$, polarization charges dP/dx , and residual impurities,

which we set $3.0 \times 10^{15} \text{ cm}^{-3}$ as measured for ZnO grown under similar conditions.³³ We used a temperature of 850 °C same as the growth temperature to describe thermally populated carriers. As boundary conditions, we assumed an arbitrary value of conduction band pinning level of 1.5 eV and a flat band in the substrate region.

The calculated results are shown in Fig. 3 for Sample A, Sample E, and Sample F by using both the design and experimentally obtained SIMS Mg profiles. In Sample A, the potential of MgZnO layer slowly increases towards the surface, and the polarization mismatch ΔP is compensated by accumulating electrons of the density of $\sim 10^{19} \text{ cm}^{-3}$ as shown in the third panel from the top. The conduction band edge touches the Fermi level at the interface, and the electrons are degenerate. As a result, no atomic reconstruction occurs with maintaining the band profile close to design.

By now involving the *p*-type interface inclusive heterostructures, we contrast two cases of Sample E and Sample F. In sample E, a nearly equivalent density of electrons is accumulated at the bottom *n*-type interface compared with Sample A. In the 10 nm-thick ZnO layer of Sample E, the number of holes at the bottom interface is about one order of magnitude smaller than electrons at the top interface. In this case, only electronic reconstruction without atomic reconstruction occurs at both *p*-type and *n*-type interface because the ZnO layer is thin. Therefore, the experimental Mg distribution resembles closely the designed structure. When the capping ZnO layer is thicker as in Sample F, the *p*-type interface should similarly be reconstructed by some means. While the calculation of the designed structure for Sample F shows that electronic reconstruction by accumulating holes would relax the potential divergence, the experimental results invoke stark contrast. As discussed above, experimentally, it is found that Mg distribution is significantly modified. Utilizing the measured

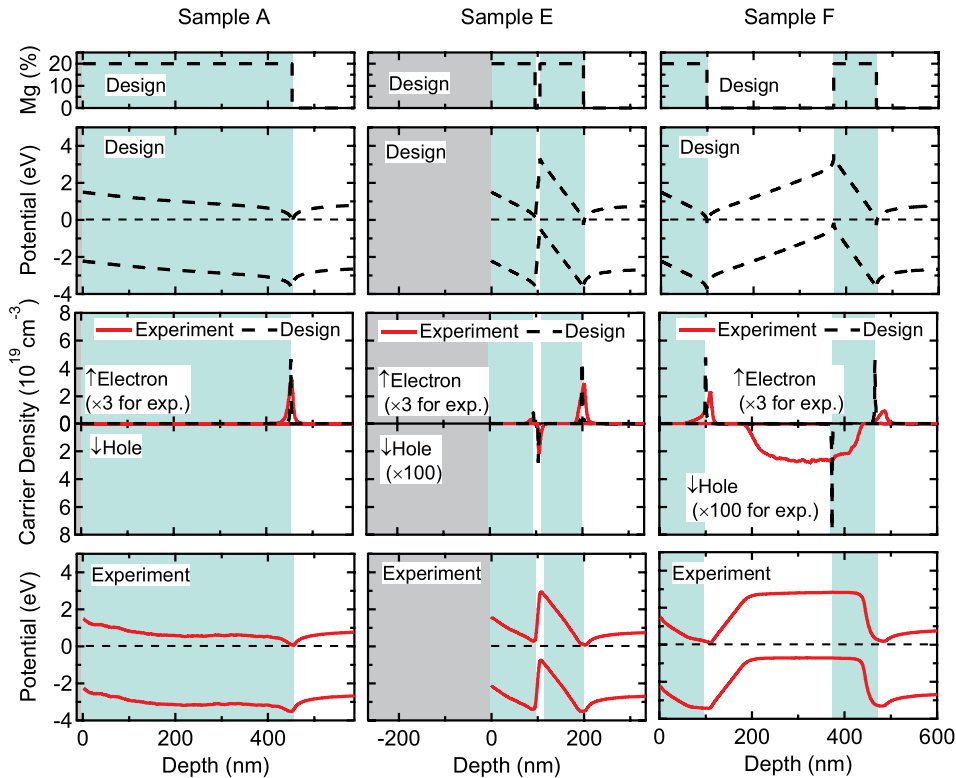


FIG. 3. For Sample A, Sample E, and Sample F: (top row panels) Designed Mg profiles, (second row panels) calculated band profiles from the designed Mg profiles, (third row panels) electron and hole distributions for the designed and experimentally detected Mg profiles, and (bottom row panels) calculated band profiles from experimentally detected Mg profiles. The calculated electron and hole densities are magnified by a factor indicated in the panels.

experimental Mg distribution in the calculation indicates that the potential profile is nearly flat in the wide range of the 300 nm-thick Mg-redistributed ZnO layer and a portion of the bottom MgZnO layer, where low density non-degenerate holes compensate polarization charges. Based on this calculation, it is apparent that Mg redistributes at the *p*-type interface as if the system aims to avoid accumulating high density holes. This fact may suggest atomic reconstruction is energetically more favorable than electronic reconstruction in the *p*-type interface, and the opposite is true of *n*-type interface. This asymmetry may be interpreted as an inherent difference in creating electrons and holes in ZnO. Although the above consideration gives a qualitative explanation for the Mg redistribution, quantitative aspects such as length scale of Mg redistribution are not clear at the moment, for example, to account for the difference of Mg distributions between Sample D and Sample F. To achieve further quantitative understanding, it may be necessary to properly include microscopic mechanism of electron-hole asymmetry as well as the effect of finite thermal diffusion.

It is worth mentioning that in contrast to the present study, previous reports of MgZnO/ZnO heterostructures and superlattices did not show any signature of atomic reconstruction or, if at all, showed only polarity-independent thermal diffusion.^{34,35} In addition to using lattice mismatched substrate such as Al₂O₃, this is probably due to the unintentional incorporation of a high density of impurities or charged defects like Zn interstitials or oxygen vacancies, which, in turn, may easily compensate the polarization charges.³⁶ In contrast, our MgZnO/ZnO heterostructures fabricated on high-purity ZnO substrates by MBE contain a small number of residual electrons of $\sim 1 \times 10^{15} \text{ cm}^{-3}$ for ZnO and $\sim 2 \times 10^{14} \text{ cm}^{-3}$ for Mg_{0.2}Zn_{0.8}O as reported from our group (Ref. 33). Since such a small number of residual carriers are not enough to compensate the polarization mismatch at the interface, the polarization charges should be internally compensated by electronic and/or atomic reconstruction, which we reveal the former is dominant for *n*-type and the latter for *p*-type interfaces. This point may be verified by intentionally including 10^{20} cm^{-3} electrons (equivalent to residual electrons from charged impurities) in the calculation for the designed structure of Sample F (not shown), where it was found that the polarization charges are completely compensated.

In summary, we have investigated contrasting electronic and atomic reconstructions at the polarization-mismatched interfaces of MgZnO and ZnO. By measuring the Mg profile of a series of heterostructures by SIMS, we found that the Mg profile remains per design in the case of *n*-type interfaces, while significant redistribution of Mg is observed for *p*-type. This phenomenon cannot be explained by thermal diffusion exclusively since a 10 nm-thick ZnO layer flanked by thick MgZnO layers remains intact without Mg reconstruction (sample E). Simulations of band structure and carrier densities reveal that instead it is electrostatic instability caused by uncompensated polarization charges at heterointerfaces which leads to Mg diffusion. This observation requires careful consideration of this newly found reconstruction mechanism in the design and optimization of electronic and optical devices.

This work was partly supported by Grant-in-Aids for Scientific Research (S) No. 24226002 from MEXT, Japan, and by “Funding Program for World-Leading Innovative R&D on Science and Technology (FIRST)” Program from the Japan Society for the Promotion of Science (JSPS) initiated by the Council for Science and Technology Policy.

- ¹R. M. Martin, *J. Vac. Sci. Technol.* **17**, 978 (1980).
- ²R. G. Dandrea, S. Froyen, and A. Zunger, *Phys. Rev. B* **42**, 3213(R) (1990).
- ³M. Städele, J. A. Majewski, and P. Vogl, *Phys. Rev. B* **56**, 6911 (1997).
- ⁴A. Ohtomo and H. Y. Hwang, *Nature (London)* **427**, 423 (2004).
- ⁵N. Nakagawa, H. Y. Hwang, and D. A. Muller, *Nat. Mater.* **5**, 204 (2006).
- ⁶H. Yamada, M. Kawasaki, T. Lottermoser, T. Arima, and Y. Tokura, *Appl. Phys. Lett.* **89**, 052506 (2006).
- ⁷J. Chakhalian, J. J. W. Freeland, H.-U. Habermeier, G. Cristiani, G. Khaliullin, M. van Veenendaal, and B. Keimer, *Science* **318**, 1114 (2007).
- ⁸O. Ambacher, J. Smart, J. R. Shealy, N. G. Weimann, K. Chu, M. Murphy, W. J. Schaff, L. F. Eastman, R. Dimitrov, L. Wittmer, M. Stutzmann, W. Rieger, and J. Hilsenbeck, *J. Appl. Phys.* **85**, 3222 (1999).
- ⁹A. Tsukazaki, A. Ohtomo, T. Kita, Y. Ohno, H. Ohno, and M. Kawasaki, *Science* **315**, 1388 (2007).
- ¹⁰A. Malashevich and D. Vanderbilt, *Phys. Rev. B* **75**, 045106 (2007).
- ¹¹J. Jerphagnon and H. W. Newkirk, *Appl. Phys. Lett.* **18**, 245 (1971).
- ¹²T. Yao and S.-K. Hong, *Oxide and Nitride Semiconductors* (Springer, Berlin, 2009).
- ¹³S. C. Abrahams and J. L. Bernstein, *Acta Cryst. B* **25**, 1233 (1969).
- ¹⁴D. Kobayashi, R. Hashimoto, A. Chikamitsu, H. Kumigashira, M. Oshima, T. Ohnishi, M. Lippmaa, K. Ono, M. Kawasaki, and H. Koinuma, *J. Electron Spectrosc. Relat. Phenom.* **144–147**, 443 (2005).
- ¹⁵A. Tsukazaki, A. Ohtomo, T. Onuma, M. Ohtani, T. Makino, M. Sumiya, K. Ohtani, S. F. Chichibu, S. Fuke, Y. Segawa, H. Ohno, H. Koinuma, and M. Kawasaki, *Nat. Mater.* **4**, 42 (2005).
- ¹⁶K. Nakahara, S. Akasaka, H. Yuji, K. Tamura, T. Fujii, Y. Nishimoto, D. Takamizu, A. Sasaki, T. Tanabe, H. Takasu, H. Amaike, T. Onuma, S. F. Chichibu, A. Tsukazaki, A. Ohtomo, and M. Kawasaki, *Appl. Phys. Lett.* **97**, 013501 (2010).
- ¹⁷H. Kato, T. Yamamoto, A. Ogawa, C. Kyotani, and M. Sano, *Appl. Phys. Express* **4**, 091105 (2011).
- ¹⁸J. S. Liu, C. X. Shan, H. Shen, B. H. Li, Z. Z. Zhang, L. Liu, L. G. Zhang, and D. Z. Shen, *Appl. Phys. Lett.* **101**, 011106 (2012).
- ¹⁹J. C. Fan, K. M. Sreekanth, Z. Xie, S. L. Chang, and K. V. Rao, *Prog. Mater. Sci.* **58**, 874 (2013).
- ²⁰X. Y. Liu, C. X. Shan, C. Jiao, S. P. Wang, H. F. Zhao, and D. Z. Shen, *Opt. Lett.* **39**, 422 (2014).
- ²¹A. Tsukazaki, A. Ohtomo, D. Chiba, Y. Ohno, H. Ohno, and M. Kawasaki, *Appl. Phys. Lett.* **93**, 241905 (2008).
- ²²A. Tsukazaki, S. Akasaka, K. Nakahara, Y. Ohno, H. Ohno, D. Maryenko, A. Ohtomo, and M. Kawasaki, *Nat. Mater.* **9**, 889 (2010).
- ²³M. Nakano, A. Tsukazaki, A. Ohtomo, K. Ueno, S. Akasaka, H. Yuji, K. Nakahara, T. Fukumura, and M. Kawasaki, *Adv. Mater.* **22**, 876 (2010).
- ²⁴J. Falson, D. Maryenko, Y. Kozuka, A. Tsukazaki, and M. Kawasaki, *Appl. Phys. Express* **4**, 091101 (2011).
- ²⁵Y. Kozuka, A. Tsukazaki, and M. Kawasaki, *Appl. Phys. Rev.* **1**, 011303 (2014).
- ²⁶K. Maeda, M. Sato, I. Niikura, and T. Fukuda, *Semicond. Sci. Technol.* **20**, S49 (2005).
- ²⁷S. Akasaka, K. Nakahara, H. Yuji, A. Tsukazaki, A. Ohtomo, and M. Kawasaki, *Appl. Phys. Express* **4**, 035701 (2011).
- ²⁸Y. Nishimoto, K. Nakahara, D. Takamizu, A. Sasaki, K. Tamura, S. Akasaka, H. Yuji, T. Fujii, T. Tanabe, H. Takasu, A. Tsukazaki, A. Ohtomo, T. Onuma, S. F. Chichibu, and M. Kawasaki, *Appl. Phys. Express* **1**, 091202 (2008).
- ²⁹Y. Kozuka, J. Falson, Y. Segawa, T. Makino, A. Tsukazaki, and M. Kawasaki, *J. Appl. Phys.* **112**, 043515 (2012).
- ³⁰S. Birner, T. Zibold, T. Andlauer, T. Kubis, M. Sabathil, A. Trellakis, and P. Vogl, *IEEE Trans. Electron Devices* **54**, 2137 (2007).
- ³¹C. Kittel and H. Kroemer, *Thermal Physics*, 2nd ed. (Freeman, New York, 1980).
- ³²P. Harrison, *Quantum Wells, Wires and Dots*, 2nd ed. (John Wiley & Sons, Chichester, 2005).

³³S. Akasaka, K. Nakahara, A. Tsukazaki, A. Ohtomo, and M. Kawasaki, [Appl. Phys. Express](#) **3**, 071101 (2010).

³⁴A. Ohtomo, R. Shiroki, I. Ohkubo, H. Koinuma, and M. Kawasaki, [Appl. Phys. Lett.](#) **75**, 4088 (1999).

³⁵L. L. Yang, Q. X. Zhao, G. Z. Xing, D. D. Wang, T. Wu, M. Willander, I. Ivanov, and J. H. Yang, [Appl. Surf. Sci.](#) **257**, 8629 (2011).

³⁶S. J. Pearton, J. C. Zolper, R. J. Shul, and F. Ren, [J. Appl. Phys.](#) **86**, 1 (1999).